acta phys. slov. 43 (1993), No. 5, 333–344

DYNAMICS AND MASS YIELD DISTRIBUTION OF HIGH-ENERGY NUCLEUS-NUCLEUS COLLISION

M. Shalaby[1]

Physics Department, Faculty of Science, Ain Shams University, Abbassia-Cairo, Egypt

H. Khalil

Physics Department, College for Girls, Ain Shams University, Heliopolis-Cairo. Egypt

S.K. Hindawi, E.A. Gomaa

Physics Department, Faculty of Science, Ain Shams University, Abbassia-Cairo, Egypt

Received 14 July 1992, in final form 18 March 1993
Accepted 26 March 1993

Dynamics of high energy nucleus-nucleus collision and fragment production are studied in terms of a two-step model. The first (fast) step was described in terms of (i) Glauber multiple scattering formalism that incorporates the proper nucleus-nucleus thickness function (ii) Exponential and scaling (excitation) energy distributions during the course of collision. In the second (slow) step, we considered a simple evaporation chain for the decay probability of the high excited nucleus into fragments. Finally we arrived at a "parameter free" analytical expression for the mass yield distribution that was reasonably comparable (above mass 100) with experimental data for nucleus-nucleus collision.

I. INTRODUCTION

During the last decade, phenomenological theories of high energy nucleus- nucleus collisions have gradually been superseded by more microscopic approaches [1]. For comprehensive review of the developments in this field we refer to the work of Hufner [2], Bondorf [3], and Gross [4]. However, as a kind of guide line, classification for the mass yield distribution of the collision product fragments usually distinguishes three mechanisms: spallation, fission and multifragmentation [2].

[1]E-mail address : *SHAMS_SC@EGERCUVX.BITNET*

Spallation leads to fragments with mass number A_f close to that of target nucleus A_T, $A_f > \frac{2}{3} A_T$ and it is rather well established that it takes place when the residual nucleus formed after the course of collision has relatively low excitation energy (peripheral collision). For heavy target nuclei, fission leads to fragments with A_f around $A_T/2$ with the lighter fragments said to originate from multifragmentation. These two mechanisms are rather violent as they require a considerable amount of excitation energy deposition (central collision).

The mechanism of the high energy nucleus-nucleus collision and the associated mass yield distribution have been studied with several theoretical approaches that are based on different assumptions. Nuclear firestreak model [3] is based on the nuclear thermodynamics of Mekjian [6] and Kapusta [7]. It was assumed that there were enough interactions for thermodynamic equilibrium to occur between the nucleons that participate in the reaction. The idea in this model is similar to the one in the nuclear fireball model [8] which incorporated geometrical aspects and was used to calculate the proton inclusive spectra from relativistic heavy ion collisions. Two basic models, namely (i) the abrasion-ablation model and (ii) the intranuclear-cascade model assume that the reaction mechanism (and fragment production) proceedes in two stages.

In the abrasion-ablation approach [9,10], the two nuclei are taken to be hard spheres which move on straight line trajectory. Those nucleons in the region of the overlap of the two nuclei are sheared off in the abrasion (or fast) stage of the collision. The spectator fragments of the target (and projectile) are then assigned an excitation energy that is proportional to their excess surface energy. The primary products are then allowed to deexcite (ablation slow stage) through a statistical evaporation chain [9]. Results of this model calculations [10] reproduced the general shape for the distribution of high mass product fragments in 8.0 GeV ^{20}Ne+^{181}Ta collision [11] and overestimate the mass yield cross section by a factor of 2.

A currently used model is the Monte Carlo numerical simulation of the intranuclear cascading. In this model [12] a fast step proceeds as cascading collisions of nucleons from one reaction partner inside the nucleus of the other partner and a (slow) statistical evaporation step deexciting the primary fragments. Calculations based on numerical simulations of these events are made using the computer code [13] VEGAS for proton induced reactions which have been modified to treat two colliding nuclei. Results of this model calculation [12] predict an approximately correct general shape of nucleus-nucleus residue distribution of 8.0 GeV ^{20}Ne+^{181}Ta reaction in the region above mass number 100. However, the data and the calculations diverge below this mass number and the model does not predict the production of fragments with $A_f < 80$ in any significant amounts.

In the present work we have derived an expression for the nucleus-nucleus thickness function used in the Glauber multiple scattering theory to derive an analytical formula for the collision probability between each nucleon from the projectile with nucleons of the target nucleus. The first stage of the reaction was then described in terms of the (target) excitation function that incorporates the derived formula of collision probability with either exponential or scaling energy distributions. In the second stage we used simple evaporation chain for the decay probability of the highly excited nucleus into fragments A_f. Finally, we arrived at

a parameter free analytical expression for the mass yield distribution $\sigma(A_f)$ that is tested for the p + nucleus system (as a prerequisite) and for the nucleus + nucleus system.

II. TWO-STEP MODEL OF NUCLEUS-NUCLEUS COLLISION

In the first (fast) stage of the collision termed as heating stage, the participant nucleons from projectile A with incident energy E_p interact with nucleons of the target nucleus B. The cross-section to deposit a certain amount of energy E^* into the nucleus is considered as superposition of events with different numbers of collision ν [14], therefore,

$$\frac{1}{\sigma_R}\frac{\mathrm{d}\sigma}{\mathrm{d}E^*} = \sum_{\nu\geq 1} \sigma(\nu, AB)\, F_\nu(E^*) \tag{1}$$

where σ_R is the total reaction cross section, $\sigma(\nu, AB)$ is the cross section for the (individual) projectile nucleons to collide with ν (separate) nucleons of the target nucleus, and $F_\nu(E^*)$ is the probability that the nucleus has an excitation energy E^* as a result of the collision of the projectile with ν of the target nucleons. In the second (slow) stage, of the reaction, the prefragments which are excited decay to the observed particle stable fragment nuclei. A simple evaporation chain could be used for the analytical description of this stage.

A. First (Fast) Stage of the reaction

In describing this stage of nucleus-nucleus collision , we will be concerned with the construction of analytical expressions of the two basic quantities $\sigma(\nu, AB)$ and $F_\nu(E^*)$, in a form suitable for direct computation of $\mathrm{d}\sigma/\mathrm{d}E^*$.

A.1. Collision probability : $\sigma(\nu$,AB)

In an inelastic collision between a nucleus with mass number A and a nucleus with mass number B, the probability for the occurrence of ν inelastic nucleon-nucleon collision at an impact parameter b is given by [15],

$$\sigma(\nu, AB) = \frac{\int \mathrm{d}^2\mathbf{b}\binom{AB}{\nu}\,[Y_{AB}(\mathbf{b})]^\nu[1-Y_{AB}(\mathbf{b})]^{AB-\nu}}{\int \mathrm{d}^2\mathbf{b}[1-[1-Y_{AB}(\mathbf{b})]^{AB}]} \tag{2}$$

where $Y_{AB} = \sigma_{in}T_{AB}(\mathbf{b})/AB$ is the probability that a given nucleon of A collides with a given nucleon of B, σ_{in} is the total nucleon-nucleon inelastic cross-section for particle production and $T_{AB}(\mathbf{b})$ is the thickness function for the nucleus-nucleus collision . The denominator of eq. (2) is the Glauber total reaction cross section [16]:

$$\sigma^R_{AB} = \int \mathrm{d}^2\mathbf{b}[1-[1-Y_{AB}(\mathbf{b})]^{AB}]. \tag{3}$$

The mean number of nucleus-nucleus collisions $\langle\nu_{AB}\rangle$ is given by

$$\langle\nu_{AB}\rangle = \sum_\nu \nu\sigma(\nu, AB) = AB\sigma_{in}/\sigma^R_{AB}. \tag{4}$$

The thickness function for nucleus-nucleus collision $T_{AB}(\mathrm{b})$ is given by :

$$T_{AB}(\mathrm{b}) = \int \rho_A(\mathbf{b}_A, Z_A)\rho_B(\vec{b}_B, Z_B)t(\mathbf{b}_B - (\mathbf{b}+\mathbf{b}_A)\mathrm{d}^2\mathbf{b}_A\mathrm{d}Z_A\mathrm{d}^2\mathbf{b}_B\mathrm{d}Z_B, \quad (5)$$

where ρ_A (or ρ_B) is the normalized density distribution for the nucleus A (or B), and $t(\mathbf{b})$ is the normalized thickness function for nucleon-nucleon collision.

$$\int \rho_A(\vec{r})\mathrm{d}\vec{r} = \int \rho_B(\vec{r})\mathrm{d}\vec{r} = \int T_{AB}(\mathbf{b})\mathrm{d}^2\mathbf{b} = \int t(\mathbf{b})\mathrm{d}^2\mathbf{b} = 1 \quad (6)$$

The spatial coordinates $\mathbf{b}_A$, Z_A (or $\mathbf{b}_B, Z_B$) are measured with respect to the centre of the nucleus A or B. The thickness function $T_{AB}(\mathbf{b})$ (and consenquently the collision probability $\sigma(\nu, AB)$) could be formulated for different nuclear density distributions. Preliminary computations of $\sigma(\nu, AB)$, considering Gaussian distribution for either of the two nuclei (A, B), shows no significant differences compared with the use of a more realistic (normal) density distribution.

$$\rho_{A,B}(\vec{r}) = C_{A,B}\, e^{-r^2/\beta^2_{A,B}};\ t(\mathbf{b}) = \frac{1}{\pi\beta_p^2}\, e^{-(\mathbf{b}_B-(\mathbf{b}+\mathbf{b}_A))^2/\beta_p^2}, \quad (7)$$

where $\beta_A^2 = (\bar{r}_0)\ A^{2/3}/3$ (or similarly β_B^2), $\beta_p = 0.68$ fm, $\bar{r}_0$ is the r.m.s. radius of the nucleus, $C_A = A/(\pi\beta_A^2)^{3/2}$ (or similarly C_B) [17], substituting in eq. (5), we get :

$$T_{AB}(b) = \frac{AB}{\pi\beta^2}\, e^{-b^2/\beta^2}, \quad \text{where } \beta^2 = \beta_A^2 + \beta_B^2 + \beta_p^2. \quad (8)$$

Analytical formula for the collision probability $\sigma(\nu, AB)$ could be directly derived using equations (8) and (2) as :

$$\sigma(\nu, AB) = \frac{1}{\nu!}\, \frac{(\nu-1)![1 - e^{-c\sigma_{in}} \sum_{s=0}^{\nu-1} \frac{(c\sigma_{in})^s}{s!}]}{E_1(c\sigma_{in}) + \ln(c\sigma_{in}) + \gamma} \quad (9)$$

where $\gamma = 0.5772156649$ is the Euler-Mascherani-constant and :

$$c = AB/(\pi\beta^2).$$

A.2. Excitation energy distribution after ν collisions: $F_\nu(E^*)$.

In each collision between the projectile and a target nucleon an energy E^* is transferred from the projectile to the target nucleus. A function $F_\nu(E^*)$ could be defined as the excitation energy distribution after ν collisions. Two possible forms will be used for this function, namely exponential distribution and scaling distribution.

Exponential distribution :

For projectile with incident energy E_p, that collides with ν target nucleons independently, the exponential distribution of energy transferred was obtained [14] by folding :

$$F_1(E^*) = \frac{1}{E_0}\ \exp[-\frac{E^*}{E_0}],$$

ν times, to give

$$F_\nu(E^*) \ = \ \frac{1}{(\nu-1)!}\ \frac{E^{*(\nu-1)}}{E_0^\nu}\ \exp[-\frac{E^*}{E_0}] \quad (10)$$

where the mean energy transfered in the collision.

$$E_0(E_p) \cong \frac{E_p}{\langle\nu\rangle}\ [1 - \exp\ (-\frac{\langle\nu\rangle}{4})] \quad (11)$$

Scaling distribution :

We consider internuclear cascade collisions in which the output spectrum from one collision is taken to be the input to the next collision. Elasticity x of the leading nucleon is defined as the ratio of the outgoing nucleon energy to its incident energy. For the case of flat spectrum in nucleon-nucleon collision the cascade spectra could be evaluated analytically to give "Distribution function of x after ν cascade collisions", denote as $F_\nu(x)$ [19]

$$F_\nu(x) = \frac{1}{(\nu-1)!}\ [-\ln x]^{\nu-1} \quad \text{where} \quad \nu > 1\,. \quad (12)$$

A prerequisite to the meaningful application of these distributions for nucleus-nucleus collision, are their application to the more simplified case of nucleon-nucleus collision. A detailed and successful treatment of nucleon (proton)-nucleus collision using the exponential distribution [14] yields the following form of the excitation function $\frac{1}{\sigma_R}\frac{\mathrm{d}\sigma}{\mathrm{dE}^*}$:

$$\frac{1}{\sigma_R}\frac{\mathrm{d}\sigma}{\mathrm{d}E^*} = \frac{1}{(\langle\nu\rangle - E_0)}\ \exp(-\frac{E^*}{(\langle\nu\rangle - 1)E_0})\,. \quad (13)$$

Also, we have derived the corresponding expression for $\frac{1}{\sigma_R}\frac{\mathrm{d}\sigma}{\mathrm{dE}^*}$ using the scaling distribution as

$$\frac{1}{\sigma_R}\frac{\mathrm{d}\sigma}{\mathrm{dE}^*} = \frac{1}{(\langle\nu\rangle - 1)}\ [\exp\ (-\frac{(\langle\nu\rangle - 1)}{\langle\nu\rangle}\ln x\ ) - 1]\,. \quad (14)$$

Computational results of the above two expressions (Eqs. 13, 14) are compared with the corresponding intranuclear cascade calculations of the excitation function available for p+ ^{159}Tb at $E_p = 0.6$ GeV [20]. As shown in Fig. 1 use of either of the two distributions is equally reasonable. The important feature to be noted is that : scaling energy distribution allows for more probable excitation of the target

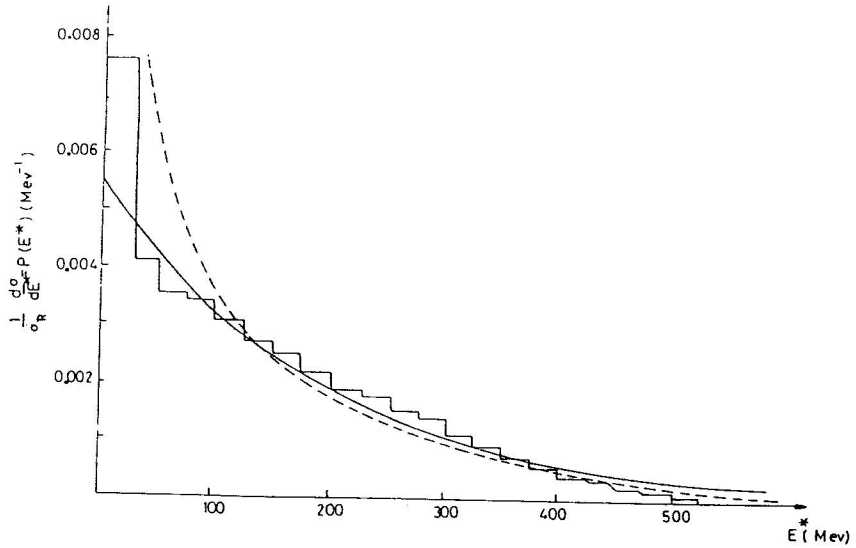

Fig. 1. The distribution of excitation energy E^* in proton - ^{159}Tb collisins at $E_p = 600$ MeV. The histogram is the result of an intranuclear cascade calculations [20]. The solid and dashed lines are the computation results of the derived analytical formula (13) and (14) using exponential and scaling distributions.

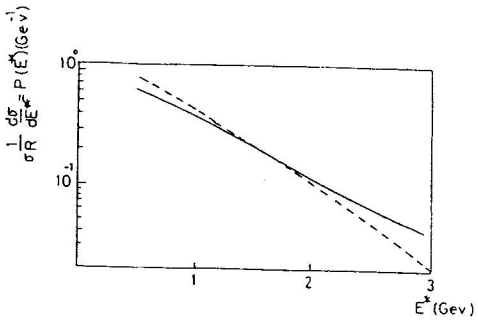

Fig. 2. The distribution of excitation energy E^* in p + ^{197}Au collision at $E_p = 3$ GeV. The solid and dashed lines are the computation results of the derived analytical formula (13) and (14) using exponential and scaling distributions respectively.

nucleus with relatively low excitation energy compared with that obtained using exponential distribution. This might strongly affects the "spallation" cross section of the mass yield distribution, where the spallation mechanism requires low excitation energy. In view of the available p+ ^{197}Au mass yield data at $E_p = 3$ GeV and 6 GeV [21], we have found it convenient to display the excitation function for this reaction at these relatively higher energies. As shown in Fig. 2, the excita-

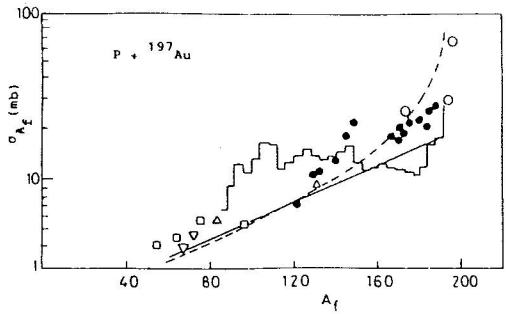

Fig. 3. Mass-Yield distribution [21] at energy 3 GeV. Histogram is the result of a cascade-evaporation calculation [23]. The solid and dashed lines are the predictions of the present two-step model calculations by using exponential and scaling energy distribution respectively, where the product types are ^{103}Ru (circle), ^{95}Nb (box), ^{95}Zr (triangle) and ^{149}Tb (full circle).

tion function, follows the above mentioned behaviour that will directly explain the experimental mass yield distribution presented in section B.

B. Second (slow) stage of the reaction :

After the first step of reaction, the target nuclei present are an ensemble of nuclei with mass A_T and a distribution of excitation energy $\frac{d\sigma}{dE^*}$. A nucleus with a given excitation energy emits nucleons or light nuclei ΔA until a particle stable final fragment with mass $A_f = A_T - \Delta A$ is reached. In each step its energy is reduced by ε, therefore, it reaches a particle stable nucleus with mass number A_f if $E^* = \varepsilon.(A_T - A_f)$. If it is assumed that ε is the same at each step of the evaporation chain, then the mass yield [22] could be written as

$$\sigma(A_f) = \varepsilon \frac{d\sigma}{dE^*}\Big|_{E^*=\varepsilon(A_i - A_f)} \tag{15}$$

The cross section to produce a fragment nucleus with mass number A_f, $\sigma(A_f)$ using the exponential distribution of energy will be

$$\sigma(A_f) = \sigma_R\, \varepsilon \sum_{\nu} \frac{\sigma(\nu, AB)}{E_0} \frac{1}{(\nu-1)!} \left[\frac{\varepsilon.(A_T - A_f)}{E_0}\right]^{\nu-1} \exp\left(\frac{-\varepsilon.(A_T - A_f)}{E_0}\right). \tag{16}$$

The corresponding expression using scaling distribution of energy will be

$$\sigma(A_f) = \sigma_R\, \varepsilon \sum_{\nu} \sigma(\nu, AB) \frac{1}{(\nu-1)!} \left[-\ln \frac{\varepsilon(A_T - A_f)}{E_p}\right]^{-1} \tag{17}$$

As a preliminary justification for the above two mass yield formule we have compared their predictions with the experimental p+ ^{197}Au mass yield data [21].

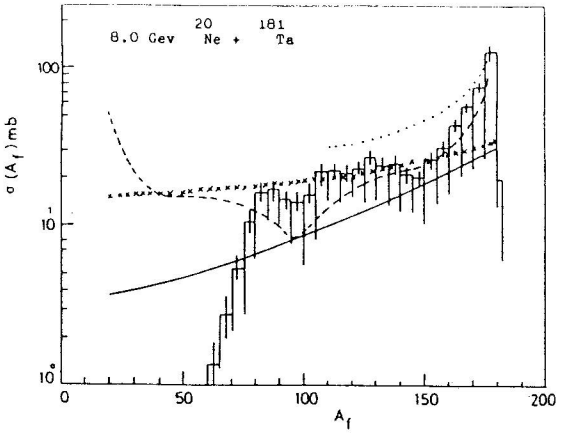

Fig. 4. A comparision of the experimental mass yield curve [11] (dashed line) with the predictions of the Monte Carlo cascade model [12] (histogram), abrasion-ablation model [9] (dotted line) and the present two-step model calculation (solid and crossed lines) using exponential and scaling energy distributions respectively.

As shown in Fig. 3, these data show an almost average increasing cross-section with increasing fragment mass A_f particularly in both fission and spallation regions. Intranuclear cascade model calculation [23] shown in Fig. 3 [as histogram] bears no resemblance to these data. The present two step model calculations closely resembles experimental data [11] particularly in considering scaling energy distribution. The pronounced rise of $\sigma(A_f)$ in the spallation region (for $A_f \geq 180$) could be well attributed to the crucial role of the excitation function (Fig. 1,2) that allows a more probable excitation of the target at relatively low excitation energy where spallation mechanism dominates. We conclude that the present (parameter free) two step model calculation, with the excitation function comprisses exponential or scaling energy distribution, together with the simple decay probability of the excited nucleus, successfully accounts for fission and spallation regions in p + nucleus collision.

III. MASS YIELD DISTRIBUTION IN NUCLEUS-NUCLEUS COLLISION:

In view of the above mentioned results, we proceed to analysis of the experimental mass yield distribution of two systems, namely (i) ^{20}Ne +^{181} Ta collision at 8.0 GeV [11] and (ii) ^{139}La+^{197}Au collision at 20.9 GeV [24], as they are comprising both light (^{20}Ne) and heavy (^{139}La) projectile collisions.

A. ^{20}Ne + ^{181}Ta collision at 8.0 GeV (^{20}Ne) energy :

The measured mass yield $[\sigma(A_f)]$ for this system [11] is shown in Fig. 4. These data are compared with predictions of (i) Monte Carlo cascade model [12], the abrasion-oblation model [9] and the present two-step model. Results of the numerical simulation (Monte Carlo) of this reaction using intranuclear cascade model [12] are shown as histogram in Fig. 4. The associated uncertainties reflect the uncertainties in the statistics of the calculations and not the uncertainties in the averages. The model was relatively successful in predicting the general shape of $\sigma(A_f)$ in the spallation region. However, below mass number 100 data and model calculations diverge and they do not predict production of nuclei with mass number less than 80 in any significant amounts. Results of the abrasion-oblation model [9] are shown in Fig. 4 as dotted line. The calculations arbitrarily cut off at $A_T \approx 110$, as products with lower mass number arise from collisions, in which the hard sphere projectile nucleus drills a cylindrical hole through the target nucleus. It is doubtful whether such nuclei are created and should be considered rather as a region outside the limitations of the original model [10]. However, even with these limited calculations ($A_f \geq 110$) the cross section is overestimated by a factor of about 2 and it is just the "general" shape of the distribution of high mass products that was reproduced. Results of the present two-step model calculations has realized considerable progress in describing data of this system for production of heavy, medium and light fragments down to mass number ≈ 30.

For deeper insight in the collision dynamics of this system we refer to the crucial role of its excitation function $\frac{1}{\sigma}\frac{d\sigma}{dE^*}$ that appears in Fig. 5. One can see the relatively small contribution of the excitation function at low excitation energy in case of using "exponential" compared to "scaling" energy distribution. At higher excitation energy one finds a considerable divergence in the excitation function with higher values associated with the choice of the scaling energy distribution. These features are strongly affecting calculations of the mass yield distribution $\sigma(A_f)$ and explain how the calculated $\sigma(A_f)$ using exponential energy distribution underestimates production of relatively light fragments with $A_f \leq 50$.

As a further justification to the present model calculations we have compared the "total" experimental cross section for production of target residues from ^{181}Ta [2.6 ± 0.4b] with the values derived from

i) the hard sphere calculations [25,26] as 3.64 b

ii) Soft sphere calculations that takes into account both the diffuseness of nuclear surface and variation of nucleon-nucleon cross section with energy [27]; as 3.47 b and

iii) The present two-step model calculations as 2.43 b; which is much closer to the experimental value.

B. ^{139}La+^{197}Au collision at 20.9 GeV (^{139}La) energy :

Experimental data of the mass yield distribution for this system [24] are shown in Fig. 6 together with a histogram representing the intranuclear cascade model calculation [12]. Although model predictions are quite satisfactory in both spallation and fission regions it does not predict production of nuclei with mass number ≤ 70, in any significant amount. As shown in Fig. 6, results of the present two-step

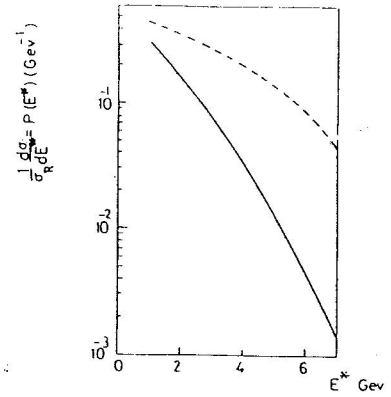

Fig. 5. The distribution of excitation energy E^* in $^{20}Ne + ^{181}Ta$ collisin at $E_p = 8.0$ GeV. The solid and dashed lines are the exponential and scaling distributions respectively.

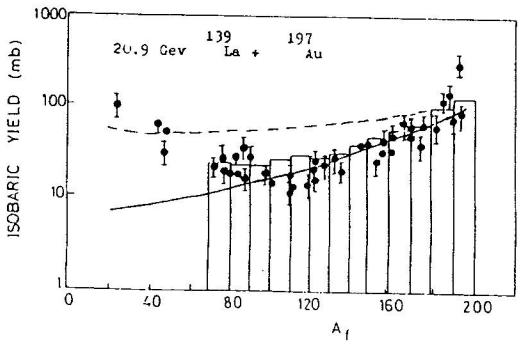

Fig. 6. A comparison of the exponential mass-yield curve [24] wit the predictions of the intranuclear cascade model [12] (histogram) and the present two-step model calculations (solid and dashed lines) using expnential and scaling energy distribution respectively.

model calculations successfully "predict" production of heavy, medium and light fragments. In view of the results using scaling energy distribution that correctly predict production of heavy and light fragments but over estimate production of medium fragments one might suggest that a proper excitation energy distribution is needed. A suggested solution to this problem might probably involve some parameters that contradicts our basic aim for a parameter free two-step model calculations.

CONCLUSION

High energy nucleus-nucleus collision mechanism and the associated mass yield distribution of product fragments (above mass 100) could be reasonably understood in terms of "parameter free" two-step model calculations. The first step of the reaction termed as "target heating" is well described by an excitation function that incorporates proper collision probability (between projectile and target nucleons) and either of the competitive exponential or scaling energy distributions. They offer a deep insight about the crucial role of this heating stage. In the second step, the target "disassemble" into fragments. The general shape and absolute cross section of high energy nucleus-nucleus collision are well produced. However, a better description to the yield of the collision fragments reveals the need for a more sophisticated treatment of the heating stage.

REFERENCES

[1] *Heavy-ion collision Cargese*, Ed. by P. Banche, M. Levy, P. Quentin, D. Varetherin, NATO ASI Series B Physics vol 130 Plenum Press.

[2] J. Hufner : Phys. Rep. *125* (1985), 129.

[3] J. P. Bondorf : Nucl. Phys. A*488* (1988), 31c.

[4] D. H. E. Gross : Rep. Progr. Phys. *53* (1990), 605.

[5] J. Gosset , J. I. Kapusta , G. D. Westfall : Phys. Rev. C*18* (1978), 844.

[6] A. J. Mekjian : Phys. Rev. Lett. *38* (1977), 640; Phys. Rev. C*17* (1978), 1051.

[7] J. I. Kapusta : Phys. Rev. C*16* (1977), 1493.

[8] G. D. Westfall , J. Gosset , P. J. Johansen , A. M. Poshanzer , W. G. Meyer H. H. Gutbrod , A. Sandoval , R. Stock : Phys. Rev. Lett. *37* (1976); J. Gosset , H. H. Gutrod , W. G. Meyer , A. M. Poskanzer , A. Sandoval , R. Stock , G. D. Westfall : Phys. Rev. C*16* (1977), 629.

[9] D. J. Morrissey , W. R. Marsh , R. J. Otto , W. Loveland , G. T. Seaborg : Phys. Rev. C*18* (1978), 1267.

[10] J. D. Bowman , W. J. Swiatecki , C. F. Tsang : *Lawrence Berkely Laboratory Report No. LBL-2908*; J. Hufner , K. Shafer , B. Schurman : Phys. Rev. C*12* (1975), 1888.

[11] D. J. Morrissey , W. Loveland , M. de Saint Simon , G. T. Seaborg : Phys. Rev. C*21* (1980), 1783.

[12] Y. Yariv , Z. Frankel : Phys. Rev. C*20* (1979), 2227.

[13] K. Chen , Z. Frankel , G. Friedlander , J. R. Grover , J. M. Miller , Y. Shimamoto : Phys. Rev. *166* (1968), 949.

[14] A. Y. Abul-Magd , W. A. Friedman , J. Hufner : Phys. Rev. C*34* (1986), 113.

[15] J. P. Vary : Phys. Rev. Lett. *40* (1978), 295.

[16] W. Czyz , L. Maximan : Ann. Phys. (N. Y.) *52* (1969), 59.

[17] Wong Cheuk-Yin : Phys. Rev. D*30* (1984), 961 and 972.

[18] J. Miller , R. P. Hurst : *Simplified calculations of exponential integral*, Math. Tables Aids Comp. *12* (1958), 187-193.

[19] A. Goned , M. Shalaby , M. Roushdy : J. Phys. G. *11* (1985), 613.

[20] H. W. Bertini , A. M. Culkowski , O. W. Herman , N. B. Gove , M. P. Gurthrie : Phys. Rev. C*17* (1978), 1382.

[21] S. B. Kaufman , E. P. Steinberg : Phys. Rev. C*22* (198), 167.

[22] X. Campi , J. Hufner : Phys. Rev. C*24* (1981), 2199.

[23] H. W. Bertini : Phys. Rev. C*6* (1972), 631.

[24] W. Loveland , Z. Xu , C. Casey : Phys. Rev. C*38* (1988), 2094.

[25] H. L. Bradt , B. Peters : Phys. Rev. *77* (1950), 54.

[26] H. H. Heckman , D. E. Greiner , P. J. Lindstrom , H. Shwe : Phys. Rev. C*17* (1978), 1735.

[27] P. J. Karol : Phys. Rev. C*11* (1975), 1203.